

Comparison between post-smoothed maximum-likelihood and penalized-likelihood for image reconstruction with uniform spatial resolution

Johan Nuyts , Jeffrey A. Fessler

Abstract—Regularization is desirable for image reconstruction in emission tomography. One of the most powerful regularization techniques is the penalized-likelihood reconstruction algorithm (or equivalently, maximum-a-posteriori reconstruction), where the sum of the likelihood and a noise suppressing penalty term (or Bayesian prior) is optimized. Usually, this approach yields position dependent resolution and bias. However, for some applications in emission tomography, a shift invariant point spread function would be advantageous. Recently, a new method has been proposed, in which the penalty term is tuned in every pixel in order to impose a uniform local impulse response. In this paper, an alternative way to tune the penalty term is presented. The performance of the new method is compared to that of the post-smoothed maximum-likelihood approach, using the impulse response of the former method as the post-smoothing filter for the latter. For this experiment, the noise properties of the penalized-likelihood algorithm were not superior to those of post-smoothed maximum-likelihood reconstruction.

I. INTRODUCTION

Regularization of maximum-likelihood expectation-maximisation reconstruction (MLEM), by combining the likelihood with a penalty [1–6], often results in position and image dependent spatial resolution. However, for some applications in emission tomography (e.g. image analysis based on kinetic modeling or on standardized uptake values [7]), it is desirable to have uniform spatial resolution. Recently, methods have been proposed to impose uniform resolution, by combining the likelihood with a data dependent penalty [8–10] or by tuning the characteristics of a filter applied during iterations [11]. An alternative method to obtain uniform resolution is to post-smooth the reconstruction obtained after many iterations of a maximum-likelihood (ML) reconstruction algorithm [12], [13]. Applying a sufficiently high number of iterations ensures a nearly bias-free reconstruction, so after post-smoothing, the spatial resolution is uniform and the point spread function is (nearly) identical to the smoothing filter. In this paper, we first derive an approximate expression for the “natural” shape of the local impulse response function associated with a quadratic penalty term. Then, a new

penalized-likelihood method is proposed to obtain a symmetric and shift invariant point spread function. The performance of this new algorithm is compared to that of post-smoothed ML reconstruction.

II. THEORY

A. The local impulse response with the quadratic prior and uniform likelihood

Consider a one dimensional image, with pixels subject to independent Gaussian noise (with known and constant variance) and regularized with a quadratic smoothing penalty, as described by the following equations

$$L(y, \lambda) = \sum_j L_j = -\frac{1}{2} \sum_j (\lambda_j - y_j)^2 \quad (1)$$

$$P_1(\lambda) = -\frac{w}{4} \sum_j ((\lambda_j - \lambda_{j-1})^2 + (\lambda_j - \lambda_{j+1})^2) \quad (2)$$

where L is the log-likelihood and $-P_1$ the penalty, λ_j and y_j are the reconstructed and measured pixel values in j and w is the penalty weight. To study the local impulse response of the image maximizing $L + P$, we assume that the measured values for all pixels are zero, except for a single pixel α , for which it equals $A > 0$. Setting $\partial(L + P_1)/\partial\lambda_j = 0$ for a pixel with $j \neq \alpha$ produces an equation in λ_j, λ_{j-1} and λ_{j+1} . Substituting $\lambda_j = ab^j$ reveals that the equation is satisfied if

$$\lambda_j = ab^j \quad \text{and} \quad b = \frac{1 + 2w \pm \sqrt{1 + 4w}}{2w}, \quad (3)$$

where a can be determined by requiring that the sum (over all pixels) of the impulse response equals the sum of the impulse. The local impulse response has an exponential shape for this 1D problem. The same result has been derived earlier by Unser et al [14] using the z-transform representation.

A simple approximate expression for the 2D case can be obtained, under the assumption that the local impulse response is circularly symmetric, and that effects of the pixel grid can be ignored. Experience shows that circular symmetry can be achieved with good approximation using a 4 or 8 pixel neighborhood. Assume that the local impulse is centered at pixel $j = 0$, and that λ_j represents the pixel value at a distance of j pixels from the center. The average distance of

J Nuyts is with the department of Nuclear Medicine, K.U.Leuven, Herestraat 49, B3000 Leuven, Belgium, e-mail: Johan.Nuyts@uz.kuleuven.ac.be. J. A. Fessler is with the department of Electrical Engineering and Computer Science, 4240 EECS, University of Michigan, Ann Arbor, MI 48109-2122, e-mail: fessler@umich.edu. This work is supported by the grants OT/00/32 of K.U.Leuven and G.0174.03 of the Flemisch Fund for Scientific Research (FWO). J. A. Fessler’s effort was supported in part by NSF grant BES-9982349.

the neighbors of the pixel at j is larger than j . This can be taken into account by modifying the weights in (2) as follows:

$$P_2(\lambda) = -\frac{1}{4} \sum_j \left\{ w \frac{j-1+\epsilon}{j+\epsilon} (\lambda_j - \lambda_{j-1})^2 + w \frac{j+1+\epsilon}{j+\epsilon} (\lambda_j - \lambda_{j+1})^2 \right\}, \quad (4)$$

where ϵ is a small positive constant, introduced to avoid the singularity for $j = 0$. To compute the local impulse response, we proceed as above, obtaining the following solution:

$$\lambda_j \simeq \frac{a}{(j+\epsilon)} e^{-|\ln(b)|j}, \quad \text{and } b \text{ as in (3)}. \quad (5)$$

The main conclusion is that the local impulse response of the quadratic prior has an exponential shape which is rather different from that of typical low pass filters used in nuclear medicine. Comparing penalized-likelihood methods with post-filtering methods requires careful matching of the impulse responses.

B. Emission tomography

In emission tomography, the log-likelihood function can be written as [12]:

$$L(y, \lambda) = \sum_i \{y_i \ln(r_i) - r_i\} \quad (6)$$

$$r_i = \sum_j c_{ij} \lambda_j + q_i \quad (7)$$

where y_i is the measured photon count in detector i , λ_j is the radioactivity in pixel j , c_{ij} is the probability that a photon emitted in j is detected in i , q_i is the expected number of counts contributed by such processes as scatter and randoms, and terms independent of λ have been dropped. The certainty provided by the likelihood is position dependent. Combination with a uniform penalty term yields position dependent smoothing. In [8], an algorithm is presented to impose approximately uniform spatial resolution by tuning the weights w_{jk} of a quadratic penalty of the form:

$$P(\lambda) = \frac{1}{4} \sum_j \sum_k w_{jk} (\lambda_j - \lambda_k)^2, \quad (8)$$

where the weights w_{jk} are zero except when pixels j and k are neighbors, and $w_{jk} = w_{kj}$. Based on the analysis of an explicit expression for the local impulse response function, the authors proposed to chose the weights as follows:

$$w_{jk} \sim \sqrt{\left(\sum_i \frac{c_{ij}^2}{\bar{y}_i} \right) \left(\sum_i \frac{c_{ik}^2}{\bar{y}_i} \right)}, \quad (9)$$

where \bar{y}_i is the measurement mean for detector i . The factors between parentheses are the j -th and k -th diagonal elements of the Fisher information matrix [15], which can be regarded as a measure for the certainty provided by the likelihood. We will denote this algorithm as CPL, ‘‘Certainty based Penalized-Likelihood reconstruction’’. Although this algorithm makes the

resolution more uniform, the resulting local impulse response is asymmetric, and the asymmetry is still position dependent. Stayman and Fessler [9], [10] have extended the algorithm to reduce the asymmetry as well. Their approach is based on an explicit expression for the local impulse response function, and they optimize the weights w_{jk} to obtain a best fit between this computed local impulse response and a predefined target impulse response.

Here we follow a different approach, aiming at a simpler algorithm. The Fisher information estimates the ‘‘resistance’’ of the likelihood against smoothing, and with (9), more smoothing is applied if the resistance is higher. However, the Fisher information measures the certainty about the absolute pixel values, whereas the smoothing only penalizes differences between pixel values. So it seems meaningful to estimate the resistance against smoothing by computing the certainty about pixel *differences* provided by the likelihood. To do this for a particular pixel pair (j, k) , we rewrite the likelihood (6) as a function of the difference and sum of these pixels, and compute the Fisher information for estimating the difference. Setting $d_{jk} = \lambda_j - \lambda_k$, we obtain

$$w_{jk} \sim -E \left(\frac{\partial^2 L(y, \lambda)}{\partial d_{jk}^2} \right) = \frac{1}{4} \sum_i \frac{(c_{ij} - c_{ik})^2}{\bar{y}_i}, \quad (10)$$

where E is the expectation, and \bar{y}_i is the expectation of y_i . For a projection line i intersecting both pixels j and k , we have $c_{ij} \simeq c_{ik}$, so this projection i does not contribute any certainty. In contrast, a projection line perpendicular to the line connecting j and k can only intersect one of the pixels, and in that case it contributes a maximum amount of certainty. Consequently, we can introduce the following approximation:

$$\sum_i \frac{(c_{ij} - c_{ik})^2}{\bar{y}_i} \simeq \sum_{i \in S_{j-k}} \frac{c_{ij}^2}{\bar{y}_i}, \quad (11)$$

where S_{j-k} is the subset of projections with projection line approximately perpendicular to the line connecting the centers of pixels j and k .

We investigated a modified penalty for 2D reconstruction by inserting approximation (11) directly in (10), using four different subsets S_{j-k} . This approach only somewhat improved the resolution uniformity if the weights w_{jk} were computed using 8 neighbors in a 3x3 neighborhood. However, if only horizontal and vertical neighbors were used, good resolution performance in vertical and horizontal direction was observed. It seems that there is some interference between diagonal and vertical directions in the 8-neighborhood system, which is not captured by (10). This interference could be avoided by using a heuristic modification. For every pixel, we compute the ‘‘directional’’ Fisher information in vertical, horizontal and diagonal directions using (11). If the ‘‘directional’’ Fisher information (11) is maximum along a vertical or horizontal direction, then the weights of the diagonal elements are simply set to zero. If the ‘‘directional’’ Fisher information is maximum along one diagonal direction, the weights for the vertical and horizontal neighbors are set to the minimum Fisher information and that

of the other diagonal is set to zero ¹. The resulting weights are smoothed with a 2D Gaussian, and finally all weights are rescaled to ensure that the sum over all neighbors equals the sum of (11) over the four subsets. This approach aims at good performance along the four principle directions, hoping that this will suffice for acceptable performance in any direction.

This new algorithm is actually a straightforward extension of the CPL-algorithm (9). The essential difference is that in the new algorithm, the Fisher information is split in different components, which represent the information about pixel differences along different orientations. It is convenient to give it a name, so we will denote the new algorithm as OCPL, “Orientation dependent Certainty Penalized Likelihood”. After designing the penalty function with OCPL, we are ready to maximize the penalized-likelihood objective function: the sum of (6) and (8). One could apply any of the many iterative algorithms in the literature to this optimization problem. For the results given in the following section, we have applied the gradient ascent algorithm proposed in [6].

III. EXPERIMENTS

A. The shape of the local impulse response

To assess the value of the approximate equation (5), the two-dimensional uniform likelihood problem has been simulated, using an 8-pixel neighborhood, a weight of 1 for direct neighbors and of $1/\sqrt{2}$ for diagonal neighbors and a strong global weight for the penalty term. Two hundred iterations of a gradient ascent algorithm were applied. The horizontal row containing the center of the impulse response was extracted to obtain a one dimensional profile, and the three parameters of (5) were computed with least squares fitting.

B. Evaluation of the new method

The OCPL method was implemented and evaluated with two-dimensional PET and SPECT simulations. Figure 1 shows the activity distribution of the 2D software phantom. The object consists of a uniform low activity background disk containing circles of higher activity, and uniform attenuation. For the SPECT simulation, collimator blurring was taken into account (using Gaussian diffusion [16]). No noise has been added. A circle is useful to evaluate orientation dependent smoothing, since recovery of the circular activity is sensitive to smoothing in any direction. The asymmetric position of the circles ensures strong position and orientation dependence of the certainties provided by the likelihood.

Reconstructions were computed with a uniform quadratic prior, with the CPL-algorithm (9), with the new OCPL-method and with post-smoothed MLEM. For the smoothing kernel in post-smoothed MLEM, we used the impulse response of the OCPL method to ensure a good resolution match between the

¹Simply setting the vertical and horizontal weights to zero would divide the image into two independent subimages, corresponding to the white and black fields on a checkerboard. Some coupling along vertical and horizontal direction is needed.



Fig. 1. Simulation object to evaluate the new uniform resolution penalized-likelihood with PET and SPECT.

two methods. With the quadratic prior and the CPL-method, the impulse response is not symmetrical and a close match with the other methods cannot be imposed. An approximate match was achieved by tuning the penalty aiming at similar mean signal recovery along the circle. A high number of iterations was applied: 200 for PET and 450 for SPECT. We used a higher number for SPECT, because the inclusion of collimator blurring slows down convergence.

C. Comparison to post-smoothed MLEM

The aim of this experiment was to compare the signal-to-noise ratio obtained with the OCPL algorithm to that obtained with post-smoothed MLEM. In a first experiment, a simple elliptical object was used, with uniform activity and uniform attenuation. First, a single hot pixel was inserted in the image and noise-free attenuated PET-projections were computed (128 projections with 80 bins per projection). An OCPL-reconstruction was computed using 200 iterations. The very same procedure was applied again, but this time without the hot pixel. The difference between the two images is the local impulse response. This local impulse response was captured in a filter mask (15 x 15 pixels), for later use as the smoothing filter in post-smoothed MLEM.

Subsequently, two more hot pixels were inserted, and attenuated PET-projections were computed. These were used as the mean of a Poisson distribution, and 400 noise realizations were generated. In addition, 400 noise realizations in absence of the hot pixels were produced. From all these simulated projections, images were reconstructed with three different algorithms: 1) 200 iterations of the new OCPL-algorithm; 2) 200 iterations of the MLEM algorithm, followed by post-smoothing; 3) 6 iterations of iterative filtered backprojection (IFBP), followed by post-smoothing with the same impulse response. IFBP was used, because with regular (non-iterative) filtered backprojection, a small amount of smoothing due to interpolation is hard to avoid. This smoothing is eliminated after a few iterations of IFBP. After 200 iterations of MLEM or 6 iterations of IFBP, the impulse response of the unsmoothed reconstructions was very close to an ideal impulse. Consequently, after post-filtering, both reconstructions should have nearly exactly the same impulse response as the penalized-likelihood algorithm.

From the 400 noise realizations with and 400 realizations without signal, the signal-to-noise ratio in the three hot pixels is

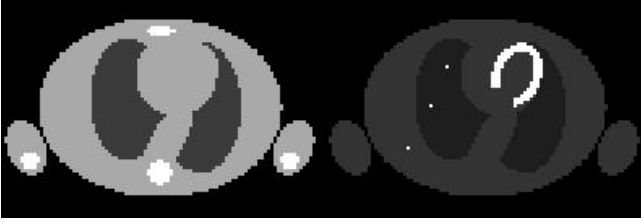


Fig. 2. Attenuation map (left) and activity distribution (right) for the simulated thorax phantom. The points are numbered from bottom to top, the first point (in tissue) is used to determine the local impulse response.

computed. For visual inspection, also the mean and variance images were computed for each of the reconstruction algorithms.

The results were verified with a simplified simulation of a PET study of the thorax, using the phantom shown in figure 2. Due to the asymmetry of the attenuation, the local impulse response function is very asymmetric if a uniform prior is used [9]. The processing of this phantom was identical to that of the first one, except that more iterations were needed to obtain sufficient convergence. We used acceleration based on ordered subsets [17], applying an iteration scheme with gradually decreasing number of subsets (16, 8, 4, 2 and 1 subset, 16 iterations of each), which is roughly equivalent to about 500 regular MLEM iterations.

IV. RESULTS

A. The shape of the local impulse response

Expression (5) was fitted to the horizontal profile, extracted from the image. An excellent fit was obtained, the fitted parameters were $a = 3.24$, $\ln(b) = 0.11$ per pixel and $\epsilon = 1.06$ pixels.

B. Evaluation of the new method

Figure 3 shows the SPECT-images obtained with the four reconstruction programs. Circumferential profiles have been computed by scanning the pixel positions on the circles in the true image (figure 1) and extracting the corresponding reconstructed pixel values. The profiles confirm that the reconstruction with OCPL is more uniform than that with the quadratic penalty and with CPL, but still not as uniform as post-smoothed MLEM. For PET, similar results were obtained, except that the uniformity was slightly better for all methods (due to lack of collimator blurring).

C. Comparison to post-smoothed MLEM

Figure 4 shows the variance and mean images computed from the 400 noise realizations, for each of the reconstruction algorithms. Because there was no non-negativity constraint in IFBP, this algorithm produces noticeable variance in the background. In the mean images, a small overshoot near the boundary of the object is seen for the OCPL-algorithm. The mean image in absence of hot pixels was subtracted from the mean image with hot pixels, to generate the local impulse responses at

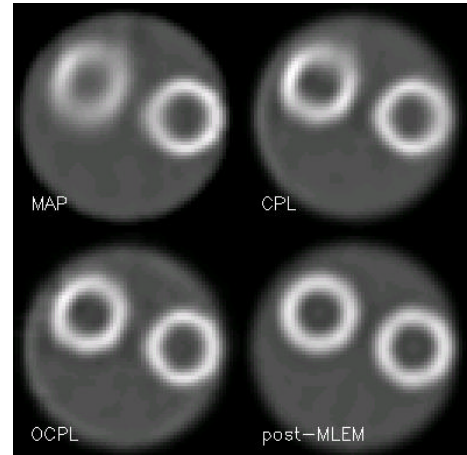


Fig. 3. The reconstructions of the SPECT simulations: the MAP-reconstruction with quadratic penalty, CPL-reconstruction, OCPL-reconstruction and post-smoothed MLEM-reconstruction.

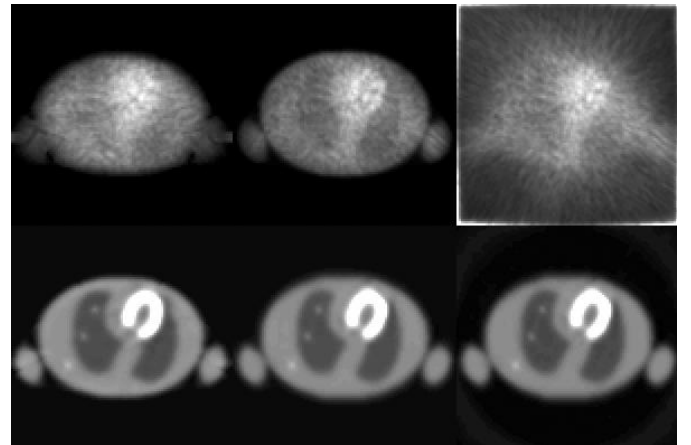


Fig. 4. The variance (top) and mean (bottom) images, computed from the 400 Poisson noise realizations for the thorax phantom. Left: OCPL-reconstruction, center: post-smoothed MLEM, right: iterative filtered backprojection.

the three hot pixel positions. For each local impulse response, four profiles (horizontal, vertical, and the two diagonal ones) were extracted by sampling along oriented straight line intervals through the center of the impulse response. We found that the profiles for the three algorithms are nearly identical in all four directions, confirming that a close match of spatial resolution was achieved.

Table I shows the signal-to-noise ratios for each of the points. In each case, point 1 was the hot pixel that was used to define the local impulse response function. The signal-to-noise ratio was best for post-smoothed MLEM, but the performance differences are relatively small and position dependent.

Finally, figure 5 compares the coefficients of variation in every pixel, for the three algorithms and for the thorax phantom. Images are produced by setting a pixel to 1 if the ratio of standard deviation and mean in that pixel is lower with one algorithm than with the other. Of course, this figure provides

TABLE I

THE SIGNAL-TO-NOISE RATIO'S FOR THE THREE POINTS IN THE MONTE CARLO SIMULATION FOR THE THREE RECONSTRUCTION ALGORITHMS (OCPL, POST-SMOOTHED MLEM AND IFBP, AND FOR THE TWO SOFTWARE PHANTOMS.

Elliptic phantom			
point	OCPL	pMLEM	IFBP
1	17.2	18.4	15.8
2	14.1	15.4	13.7
3	16.9	18.0	17.1
Thorax phantom			
point	OCPL	pMLEM	IFBP
1	4.35	4.37	4.18
2	4.34	4.63	4.35
3	4.55	4.74	4.39



Fig. 5. Comparison of the coefficient-of-variation (cov) images. Left: pixels where set when OCPL-cov was lower than post-smoothed MLEM-cov. Center: OCPL-cov lower than post-smoothed IFBP-cov. Right: post-smoothed MLEM-cov lower than post-smoothed IFBP-cov.

no information about signal recovery or signal-to-noise ratios.

V. DISCUSSION

In the simple denoising problem, the impulse response produced by the penalized-likelihood method with a quadratic prior had an exponential shape, with relatively sharp peak and wide extent. Similar shapes were reported in [18] for tomographs with ideal resolution, but the shapes change if more realistic detector blurring is taken into account. In contrast to post-smoothed MLEM, penalized likelihood offers little control over the shape of the impulse response.

Our simulation experiments confirm that the new penalized-likelihood method (OCPL) achieves nearly uniform resolution. However, its noise characteristics are slightly inferior to that of post-smoothed MLEM. Probably, the approximations made in the derivation of OCPL have resulted in somewhat degraded noise performance: with their more sophisticated method, Stayman et al. [19] obtained identical noise performance for post-smoothed MLEM and their new method. In any case, these studies suggest that post-smoothed MLEM has excellent noise characteristics, which are not improved by including the smoothing as a penalty in our penalized-likelihood methods. Moreover, the penalized-likelihood methods have a suboptimal performance near the object boundaries, in contrast to MLEM.

A very high number of iterations is required to ensure that the MLEM impulse response is small compared to that of the target resolution. As suggested by Stayman et al. [19], this may be a reason to use a penalized-likelihood approach as a kind of acceleration technique: the penalty improves the condition

number, which can be exploited to obtain faster convergence than with unregularized OSEM.

REFERENCES

- [1] S. Geman, D.E. McClure., "Statistical methods for tomographic image reconstruction," *Bull. Int. Stat. Inst.* vol 52-4, pp. 5-21, 1987
- [2] DS Lalush, EC Frey, BM Tsui, "Fast maximum entropy approximation in SPECT using the RBI-MAP algorithm," *IEEE Trans Med Imaging*, vol 19, 2000; pp. 286-294, 2000.
- [3] SJ Lee, Y Choi, GR Gindi, "Validation of new Gibbs priors for Bayesian tomographic reconstruction using numerical studies and physically acquired data," *IEEE Trans Nucl Sci* vol 46, pp. 2154-2161, 1999.
- [4] J Qi, RM Leahy, SR Cherry, A Chatziioannou, TH Farquhar, "High-resolution 3D Bayesian image reconstruction using the microPET small-animal scanner," *Phys Med Biol* vol 43, pp. 1001-1013, 1998.
- [5] S Alenius, U Ruotsalainen, "Bayesian image reconstruction for emission tomography based on median root prior," *Eur J Nucl Med* vol 24, pp. 258-265, 1997.
- [6] J Nuyts, D Bequé, P Dupont, L Mortelmans, "A concave prior penalizing relative differences for maximum-a-posteriori reconstruction in emission tomography," *IEEE Trans Nucl Sci*, vol 49, pp. 56-60, 2002.
- [7] JF Vansteenkiste, SG Stroobants, PJ Dupont, PR De Leyn, EK Verbeke, GJ Deneffe, LA Mortelmans, MG Demedts. "Prognostic importance of the standardized uptake value on (18)F-fluoro-2-deoxy-glucose-positron emission tomography scan in non-small-cell lung cancer: An analysis of 125 cases." *J Clin Oncol* vol 17, pp. 3201-3206, 1999.
- [8] JA Fessler, WL Rogers, "Spatial resolution properties of penalized-likelihood image reconstruction: space-invariant tomographs," *IEEE Trans Image Proc* vol 5, pp 1346-1358, 1996.
- [9] JW Stayman, JA Fessler, "Regularization for uniform spatial resolution properties in penalized-likelihood image reconstruction," *IEEE Trans Med Imaging* vol 19, pp 601-615, 2000.
- [10] JW Stayman, JA Fessler, "Nonnegative definite quadratic penalty design for penalized-likelihood reconstruction," *Proc. IEEE Nuc. Sci. Symp. Med. Im. Conf.*, 2001.
- [11] S Mustafovic, K Thielemans, D Hogg, P Bloomfield, "Object dependency of resolution and convergence rate in OSEM with filtering," *Proc. IEEE Nuc. Sci. Symp. Med. Im. Conf.*, 2001.
- [12] LS Shepp, Y Vardi, "Maximum likelihood reconstruction for emission tomography," *IEEE Trans Med Imaging*, vol MI-1, pp. 113-122, 1982.
- [13] J Nuyts, "On estimating the variance of post-smoothed MLEM images," *IEEE Trans Nucl Sci*, vol 49, June 2002 (in press).
- [14] M Unser, A Aldroubi, M Eden. "Recursive regularization filters: design, properties and applications," *IEEE Trans Pattern Anal Machine Intell*, vol 13, pp 272-277, 1991.
- [15] HH Barrett, JL Denny, RF Wagner, KJ Myers, "Objective assessment of image quality. II. Fisher information, Fourier crosstalk, and figures of merit for task performance," *J Opt Soc Am A* vol 12, pp. 834-852, 1995.
- [16] AW McCarthy, MI Miller, "Maximum likelihood SPECT in clinical computation times using mesh-connected parallel computers", *IEEE Trans Med Imaging*, vol 10, pp. 426-436, 1991.
- [17] MH Hudson, RS Larkin, "Accelerated image reconstruction using ordered subsets of projection data," *IEEE Trans Med Imaging* vol 13, pp. 601-609, 1994.
- [18] JA Fessler, "Spatial resolution properties of penalized weighted least-squares tomographic image reconstruction with model mismatch," Technical Report 308, Comm. and Sign. Proc. Lab., Dept. of EECS, Univ. of Michigan, Ann Arbor, MI, 48109-2122, Mar 1997.
- [19] JW Stayman, JA Fessler, "Compensation for nonuniform resolution using penalized-likelihood reconstruction in space-variant imaging systems," submitted to *IEEE Trans Med Imaging*.